Integrated Ferroelectrics
An International Journal

ISSN: (Print) (Online) Journal homepage: https://www.tandfonline.com/loi/ginf20

FBG Hydrogen Sensor Based on Pd_{87}–Ni_{13}/Pd_4–Ag_1 Thin Film and Femtosecond Laser Ablation

Xian Zhou, Joseph Muna Karanja, Mo Yang, Fei Zhou, Kefei Liu, Xingzu Ming & Yutang Dai

To cite this article: Xian Zhou, Joseph Muna Karanja, Mo Yang, Fei Zhou, Kefei Liu, Xingzu Ming & Yutang Dai (2021) FBG Hydrogen Sensor Based on Pd_{87}–Ni_{13}/Pd_4–Ag_1 Thin Film and Femtosecond Laser Ablation, Integrated Ferroelectrics, 221:1, 1-11, DOI: 10.1080/10584587.2020.1803673

To link to this article: https://doi.org/10.1080/10584587.2020.1803673

Published online: 14 Dec 2021.

INTEGRATED FERROELECTRICS
2021, VOL. 221, 1–11
https://doi.org/10.1080/10584587.2020.1803673

Taylor & Francis
Taylor & Francis Group

Spiral Microstructured FBG Hydrogen Sensor Based on Pd_{87}–Ni_{13}/Pd_4–Ag_1 Thin Film and Femtosecond Laser Ablation

Xian Zhou[a], Joseph Muna Karanja[b], Mo Yang[a], Fei Zhou[a], Kefei Liu[a], Xingzu Ming[a], and Yutang Dai[c]

[a]Institute of Mechanic Engineering, Hubei University of Arts and Science, Xiangyang, Hubei, China; [b]School of Pure and Applied Sciences, Kirinyaga University, Kerugoya, Kenya; [c]China National Engineering Laboratory for Fiber Optic Sensing Technology, Wuhan University of Technology, Wuhan, Hubei, China

ABSTRACT

A novel laser machined spiral microstructure fiber Bragg grating (FBG) hydrogen sensor and coated with composite sensing film is presented. The sensor probes are sputtered with Pd/Ni and Pd/Ag film, respectively. Experimental results exhibit that a pitch 60 μm FBG with double spiral microstructures, coated with 520 nm Pd/Ni and Pd/Ag film has hydrogen gas sensitivity in air of 13 pm/%H and 25 pm/%H, respectively. The laser-ablated spiral microstructured probes with composite films shown greater sensitivity compared with standard FBG probes with similar coating. The optimum testing temperature (50 °C) enhanced the sensitivity and repeatability of the probes.

ARTICLE HISTORY
Received 21 November 2019
Accepted 31 March 2020

KEYWORDS
Femtosecond laser; hydrogen gas sensor; spiral microgroove; fiber Bragg grating; Pd–Ni; Pd/Ag

1. Introduction

As the demand for clean energy escalates worldwide, hydrogen gas offers unparalleled green energy alternatives. However, hydrogen gas is easy to leak and explode at the limit of 4% in air. It is therefore important to detect hydrogen gas to avoid hydrogen gas leak. FBG sensor has superior characteristics compared to conventional electrochemical sensors in remote and hostile environments, such as safety, high selectivity and sensitivity, high stability and miniatured size [1]. Therefore, FBG sensor performance in gas leak detection and monitoring in distribution measurement is unparalleled.

Hydrogen gas sensors using palladium or palladium alloy thin films offer a superior sensitivity compared to pure Pd. Exposure of the sensor probe to hydrogen gas leads to surface cracking, Pd layer peeling off, and formation of blisters due to uptake and desorption of the gas due to α–β phase transition [2]. Additionally, the response time is too long for real-time hydrogen gas monitoring. Inclusion of other metals to form palladium alloy composite film such as Pd–Ni [3–7], Pd–Mg [8, 9], Pd–Au [10], Pd–Ag [11], partly reduces α–β transition and improve hydrogen uptake potential. So far, Pd/Ni alloy is one of the best candidates for hydrogen sensing due to fast responding time and reversibility. FBG hydrogen sensors based on strain have been reported in the

CONTACT Fei Zhou feidudu0521@163.com; Xingzu Ming mxz9036@126.com

literature [2]. Researchers' have explored different types of FBG hydrogen sensors such as tapered FBG sensors [12–14] and side-polished FBG sensors [15, 16] among others, improving hydrogen gas sensor probe's sensitivity and lowering response time is key to the development of FBG hydrogen sensor.

Femtosecond laser micromachining is an advanced and effective processing method, especially in the processing of transparent material domain. Hence, fs laser has been suitably utilized to fabricate microstructure on fiber resulting in making new sensors [17].

In this article, we report the fabrication and characterization of spiral micro-structured FBG hydrogen sensor coated with 520 nm Pd_{87}/Ni_{13} and Pd_4/Ag_1 thin-film, respectively. The micro-structured FBG was made by fs-laser, and the Pd_{87}/Ni_{13} and Pd_4/Ag_1 thin films were sputtered by a vacuum coating method. The hydrogen sensing characteristic of probes with two different thin films has been systematically and scientifically conducted. The effect of temperature on the sensors is also investigated.

2. Principle of Sensor

It is well known that the wavelength shift of FBG λ is a product of grating pitch Λ and effective index of fiber core Δn_{eff}, expressed as follows.

$$\lambda = 2\Delta n_{\text{eff}}\Lambda \tag{1}$$

When Pd or Pd alloy coated on the FBG absorbs hydrogen gas, the stress generated by expansion of Pd film changes the wavelength shift of FBG; thus the hydrogen concentration can be measured by monitoring the reflection or transmission spectra of the FBG. The strain will be greatly enhanced with the growing depth of microgrooves due to decrease of the fiber cross-section. The deeper the microgrooves, the more flexible is the fiber. Therefore, there needs to be a balance between fiber mechanical strength and sensitivity during sensor fabrication.

3. Experiment

The 10 mm long spiral microstructure on FBG cladding was fabricated by fs laser (780 nm, 180 fs, 1KHz). The FBG fiber was held by a highly versatile three-dimensional stage in terms of fiber rotation precision during the micro-machining process. The laser illuminated the fiber surface using a 60 mm an objective lens focal length. The laser machining activity was carried out under CCD monitoring. To achieve the intended fiber machined pitch, the fiber rotation speed ω was constant same as laser fed along the fiber axis at a uniform speed v. The laser machined spiral microstructure with a constant pitch is shown in Fig. 1. Table 1 shows the parameters of the spiral microstructures. Then, 520 nm Pd–Ni and Pd–Ag films were sputtered on the spiral micro-structured FBG using a BESTECH sputtering system. To enhance the adhesion of Pd and fiber cladding, 10 nm Ni was first sputtered. Afterwards, 520 nm Pd/Ni and Pd/Ag films were sputtered. By controlling the sputtering rate of the target, Pd–Ag films with a ratio of 4:1 and Pd–Ni films with the ratio of 87:13 were prepared. Two pieces of 5×5 mm silicon were used as a substrate to evaluate the depth and the surface

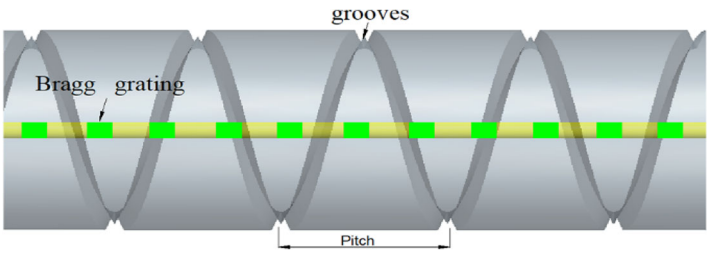

Figure 1. Schematic profile of microstructured FBG.

Table 1. Parameters of tested samples.

Specimen	Power (mW)	Pitch (μm)	Depth (μm)	Film
S-1	30	60	19	Pd_{87}/Ni_{13}
S-2	25	60	19	Pd_{87}/Ni_{13}
S-3	30	60	19	Pd_4/Ag_1
SS-1	30	60	19	Pd_{87}/Ni_{13}
SS-2	28	60	17.5	Pd_{87}/Ni_{13}
SS-3	25	60	16.5	Pd_4/Ag_1
SS-4	20	60	15	Pd_4/Ag_1
Standard FBG-a	0	0	0	Pd_{87}/Ni_{13}
Standard FBG-b	0	0	0	Pd_4/Ag_1

morphology of films. Quartz crystal method was used in real-time monitoring the thickness of the film. Finally, nine sensor probes are fabricated, as shown in Table 1.

The surface morphology and thickness of the films were measured by field emission scanning electron microscope (Zeiss Ultra Plus, Germany). The film structure was analyzed by X-ray diffraction (XRD RU-200B, Rigaku, Japan).

Hydrogen experimental facilities are composed of a gas chamber, hydrogen meter and FBG demodulator. Commercial electrochemical hydrogen calibrating meter was connected to the transparent gas chamber where the sensors were placed. Hydrogen sensors were connected to the demodulator based on CCD demodulation principle with 1 pm of testing accuracy and were tested over the range of 0–4% hydrogen concentration at room temperature and 55% of relative humidity. The demodulator port was interfaced with a computer for a real-time data collection and analysis.

4. Results and Discussion

4.1. Hydrogen Testing of $Pd_{87}Ni_{13}$ Film Sensor

Figure 2 shows the single and double spiral microstructure FBG after sputtering Pd/Ni alloy film. The designed pitch of the spiral is 60 μm while the measured pitch is ~59–61 μm. The width of micro-groove is ~17–18 μm. There is little residual debris on the surface of the cladding that does not affect the performance of the structure. Figure 3 demonstrates the image of 50 KX resolutions of the surface of Pd/Ni alloy film.

Figure 3(a,b) represents the surface morphology before and after hydrogen gas testing. The distribution of Pd and Ni particles is uniform and smooth with particle size being approximately 10-50 nm. Apparently, the thin film is blister-free. The phenomenon of film cracking and blister formation predominantly exists during hydrogen gas

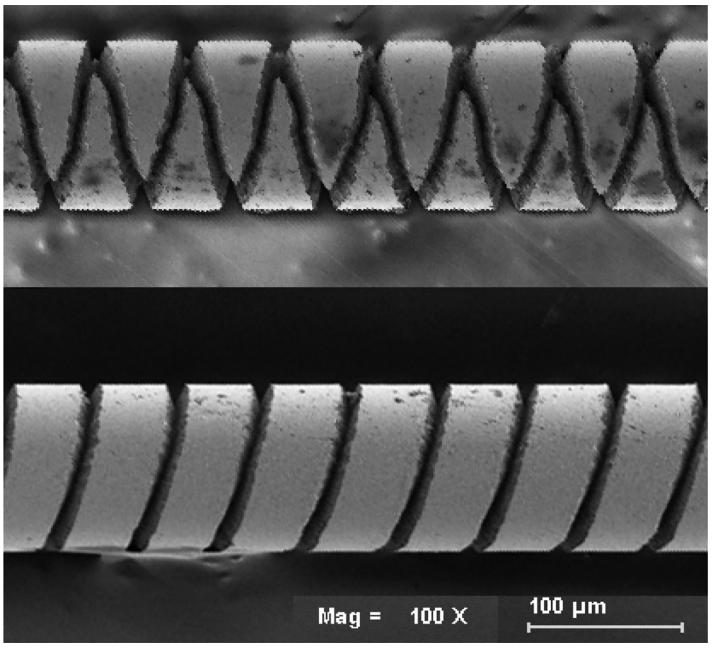

Figure 2. SEM of micro-structured FBG after sputtering Pd/Ni alloy film.

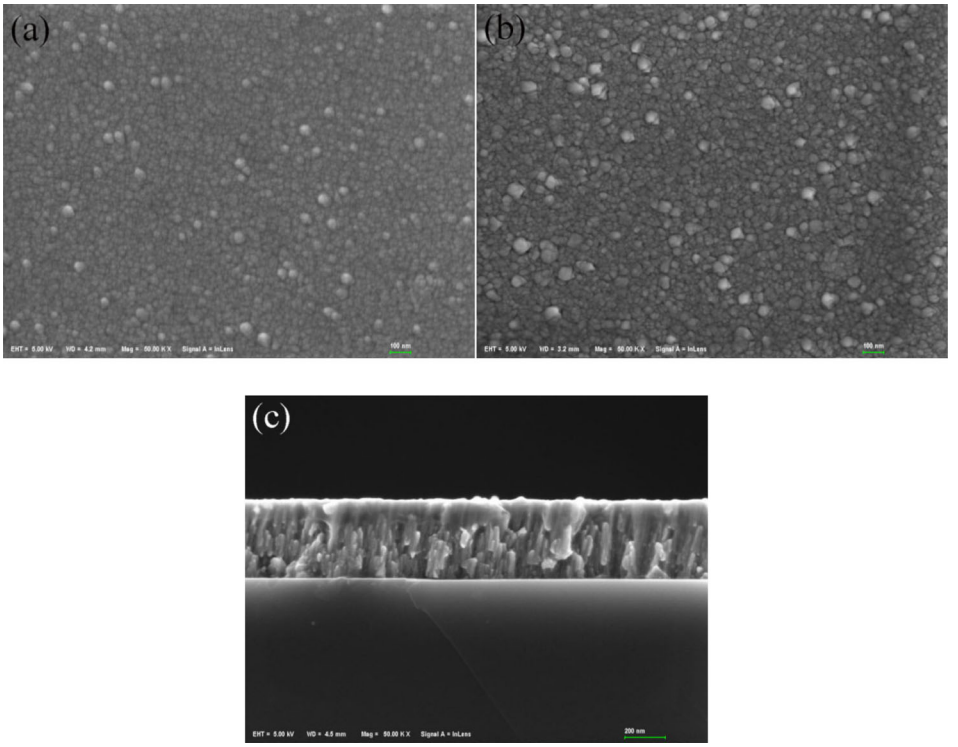

Figure 3. Surface and cross-section morphology of the film. (a) Surface morphology before hydrogen gas testing. (b) Surface morphology after hydrogen gas testing. (c) Cross section of the Pd/Ni film.

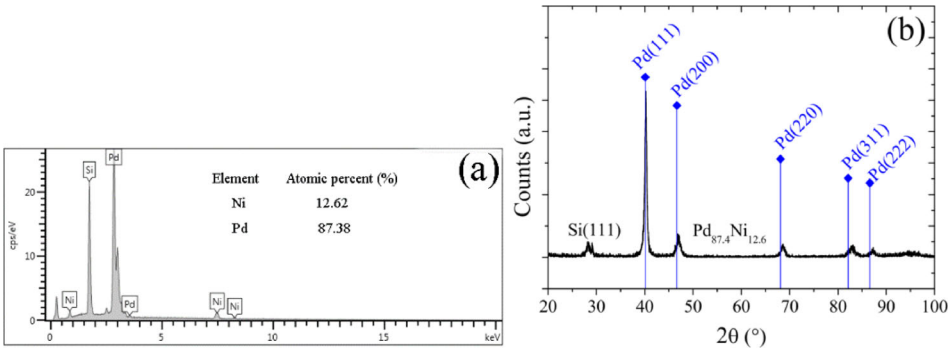

Figure 4. (a) The composition of Pd/Ni film. (b) XRD pattern of Pd/Ni film on silicon substrate.

testing of thicker pure palladium films [2]. Figure 3(b) indicates that the Pd/Ni alloy film suppressed mechanical damage and prevented the phase transition at higher hydrogen concentration. Figure 3(c) shows the cross-section of Pd/Ni alloy film on silicon substrate, and the measured depth is ~280 nm. The cross-section is composed of large particles which formed by accumulation of small particles. There are slight gaps between the thin film particles which affects the film properties such as a decrease in the density of the thin film, high dislocation density and increase residual stress. Such structural defects will affect the responding performance of the sensor. Proper Pd/Ni atoms proportional can make particles bonding stronger and thus, suppressing some structural defects. Therefore, there needs to be a balance in the alloy proportion and sensing performance. This requires us to explore further.

The elemental composition and XRD pattern of Pd/Ni film is shown in Fig. 4(a) and 4(b), respectively. The actual ratio of Pd and Ni is 6.92:1 which is consistent with the designed ratio of 7:1 (87.4:13.6). X-ray diffraction patterns of Pd/Ni film on silicon substrate were made by an X-ray diffractometer. As shown in Fig. 4(b), the peak of $2\theta = 28.46°$ is the characteristic peak of monocrystalline silicon; the square dot represents the standard XRD card data of palladium (JCPDS 46-1043). There are five characteristic peaks in the measurement of XRD diffraction spectrum. The standard peaks of Pd are $2\theta = 40.118°$, $46.658°$, $68.119°$, $82.098°$ and $86.617°$ corresponding to the cubic phase (111), (200), (220), (311) and (222) crystal planes, while the measurement data are $2\theta = 40.24°$, $46.78°$, $68.56°$, $83.42°$ and $86.74°$. Apparently, XRD peak of Pd/Ni alloy film shifts to higher degrees, which indicates that the lattice constant shrinks compared to pure Pd due to the smaller atomic radius of Ni replacing the larger Pd atoms on a FCC lattice. The XRD result illustrates the orderly arrangement of atoms in Pd/Ni alloy film.

Figure 5 demonstrates the use of air as carrier gas on three samples and their response to different concentration of hydrogen gas at ambient temperature. Hydrogen concentration ranges from 0 to 4%. The response time and recovery time are defined as the time for the sensor to reach 90% of the final equilibrium value. It is evident that the response time of ss-2 is about 80 s in Fig. 5(b) while the response time of the two other samples is about 90 s. The recovery time is shorter than response time due to the presence of air as the carrier gas. The recovery time can be enhanced in air due to consumption of the hydrogen atom by the reaction between the O^{2-} and H^{+} on the

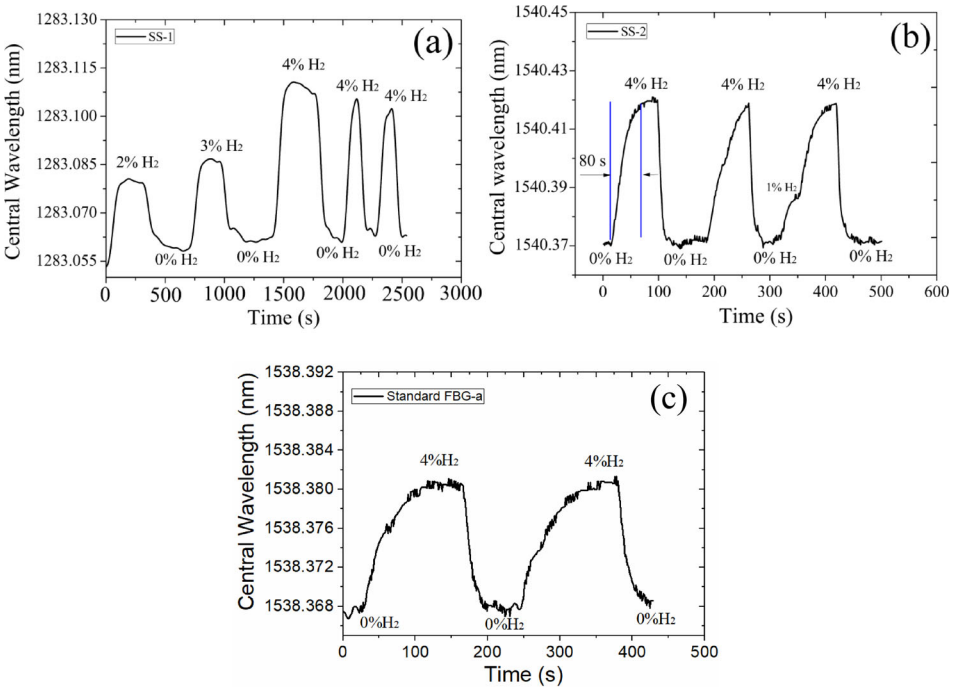

Figure 5. (a) Five cycles of sample ss-1 at different hydrogen concentration. (b) Three cycles of sample ss-2 toward 4% hydrogen concentration. (c) Hydrogen response of standard FBG-a sensor.

surface of Pd/Ni film [17]. The recovery time and response time are faster than that of probe coated Pd/Ni film with greatly etched fiber [18]. The reason may be that the larger contact area of microstructured fiber makes the sensitive membrane react with hydrogen more quickly. However, in addition to the above possible factor, the experimental ambient conditions, such as temperature, humidity and gas pressure, among others, also affect the response time.

Figure 5(a) demonstrates five cycles of hydrogen testing at different hydrogen concentrations for sample ss-1. The wavelength shift is 22, 30, 52 pm toward 2%, 3%, 4% hydrogen concentration, respectively. The central wavelength has few fluctuations after each cycle due to irreversible structural damage, although phase change can be suppressed by Ni content added to Pd film. The crystal structure of Pd/Ni cannot totally recover when the hydrogen gas is completely released.

Figure 5(b) presents sensor probe's ss-2 in terms of hydrogen response under 4% and 1% H_2 at room temperature. The sensor probes present good repeatability with the wavelength shifts being 46 and 9 pm at 4% and 1% of hydrogen concentrations respectively. As depicted in Fig. 5(c), the wavelength shift of the standard FBG-a hydrogen sensor is 7 pm at 4% hydrogen concentration.

Figure 6(a) plots the wavelength shift of duo-spiral samples machined with varying laser power and tested at different hydrogen concentrations. The laser-assisted FBG hydrogen sensors depict a linear response between 1% and 4% H_2. The hydrogen sensitivity of samples ss-1, ss-2, ss-3 and standard FBG is 13, 11.5, 8.5 and 1.75 pm/H%, respectively. Apparently, the sensitivity of the duo-spiral FBG sensor is about 7 times

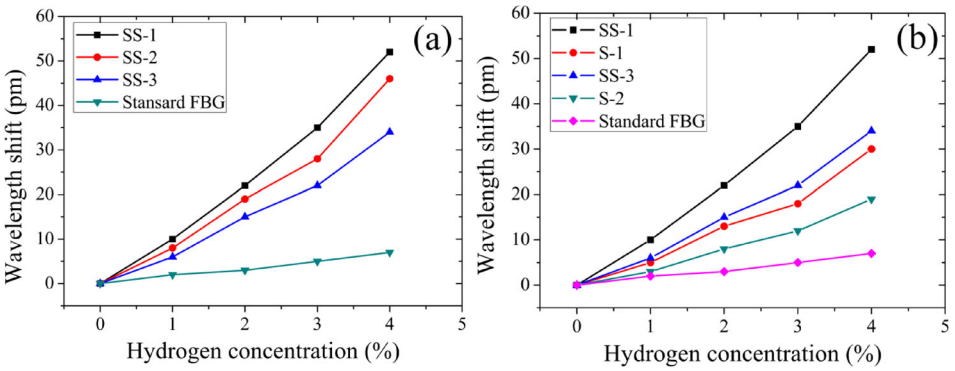

Figure 6. (a) Wavelength shift of sensors with ablated at different laser power. (b) Performance of single and double spiral sensor with same parameters.

than that of an unmutilated FBG sensor. The contributing reason being the increase of surface area and the retractability of fiber. As the larger surface area accommodates more composite particles, the palladium film expands and produces more tension. The retractability of fiber can be significantly improved due to deep microgroove on fiber cladding. Therefore, FBG sensitivity can be enhanced greatly. We also observe that the highest sensitivity sensor is ss-1, followed by ss-2 and ss-3. It indicates that higher laser energy makes the sensor more sensitive. This can be attributed to the fact that higher laser energy makes deeper grooves and with higher fiber flexibility.

Figure 6(b) shows the wavelength shift of double and single spiral sensor at different hydrogen concentrations. The sensitivities of s-1 and s-2 are 9.3 and 4.7 pm/ H%, respectively. Obviously, sample ss-1 has the highest sensitivity; the standard FBG has the lowest sensitivity. It is also found that the sensitivity of the double spiral sensor is higher than that of a single spiral sensor, for example, the hydrogen sensitivity of probe ss-1 is about 140% that of probe s-1. The reason is that the duo-spiral microstructure FBG sensor probe has increased surface area to provide increased space for the film as compared to the single spiral FBG sensor.

4.2. Hydrogen Testing of Pd_4/Ag_1 Film Sensor

Figure 7 displays hydrogen sensing results for s-3, ss-4 and standard FBG-b probes coated with 520 nm thick Pd/Ag film, conducted at room temperature, 25 °C, with carrier gas being air. Figure 7(a) demonstrates good sensor repeatability of sample s-3 in several hydrogen response cycles. The wavelength shift is about 1–2 pm higher in comparison to original samples. Figure 7(b) demonstrates hydrogen response for sample ss-4 under different hydrogen concentrations and at an ambient air condition. The wavelength shift is about 24, 87, 85 pm toward 1%, 4% and 4% of hydrogen respectively at 25 °C. Figure 7(c) shows a hydrogen gas response for a standard FBG probe under different H_2 concentrations in air condition. The central wavelength shifted between 7, 14 and 27 pm toward 1%, 2% and 4% of hydrogen concentration respectively at 25 °C. As hydrogen gas exits gas chamber, the sensor response falls back to baseline and thus, fluctuation of the central wavelength shift is about 3–4 pm. This behavior shows the sensor's reversibility property for the 1–4% hydrogen concentrations.

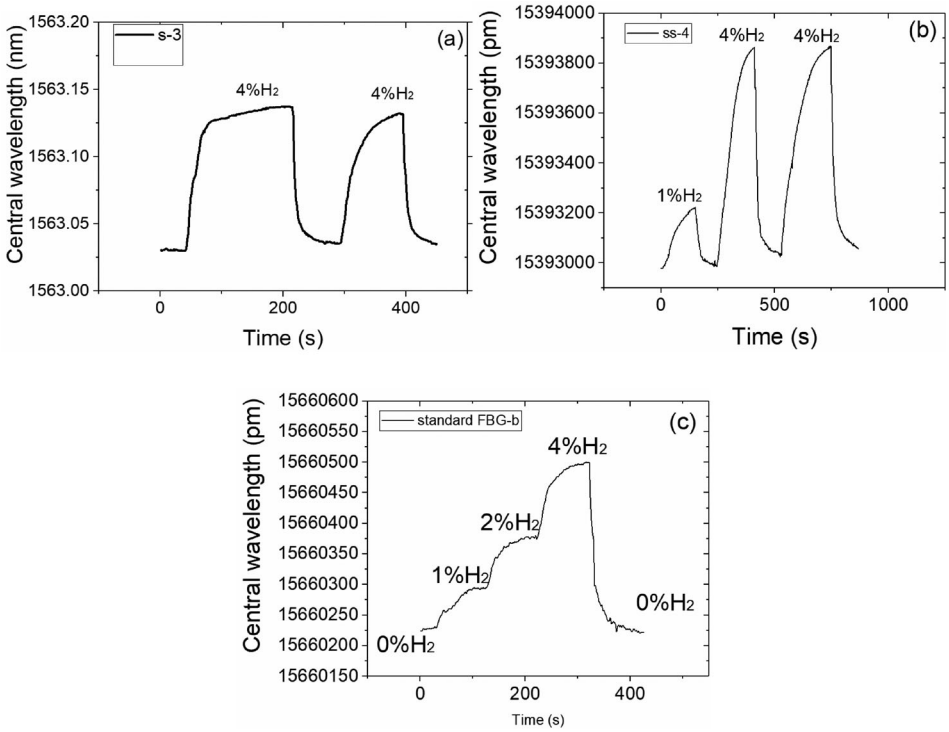

Figure 7. (a) Two cycles of sample s-3 at different hydrogen concentration both are 4%, (b) Three cycles of sample ss-4 toward different hydrogen concentration. (c) Hydrogen response of standard FBG-b sensor.

4.3. Comparing the Hydrogen Sensing Performance between the Hydrogen Sensor Coated Pd_4/Ag_1 and Pd_{87}/Ni_{13} Film

The comparison of the wavelength shift of sensor probes with different palladium alloy at 4% H_2 is shown in Fig. 8. Under the same testing conditions (laser ablation parameters and coating depth), the central wavelength of standard FBG-a and b probes shifted between 27 and 7 pm, respectively. Apparently, the wavelength shift of spiral FBG hydrogen sensor coated Pd_{87}/Ni_{13} film is lower compared to that of spiral microstructured sensors coated Pd_4/Ag_1. The reason is being that Pd, Ag and Ni are face-centred cubic structures. Their lattice constants are 0.388, 0.4 and 0.352 nm, respectively. The silver atom lattice constant is larger than that of palladium atom, again, the lattice constant of palladium atom is greater than that of nickel atom. When the Ag atom is doped into the Pd film, it forms a Pd–Ag alloy lattice structure with an enlarged lattice constant. When the Ni atom is doped into the Pd film, a new lattice structure is formed with a reduced lattice constant. Therefore, the Pd–Ag crystal lattice has more space and can absorb more hydrogen atoms, unlike the Pd–Ni nanostructures. Ultimately, the sensitivity of the probe with Pd–Ni film is lower than that of the Pd–Ag film probe.

In terms of reversibility, there is the existence of a few wavelength fluctuations Pd film during phase transition as a result of irreversible structural deformation. Doping Pd film with Ag or Ni atoms reduces the phase transition to some extent but not fully.

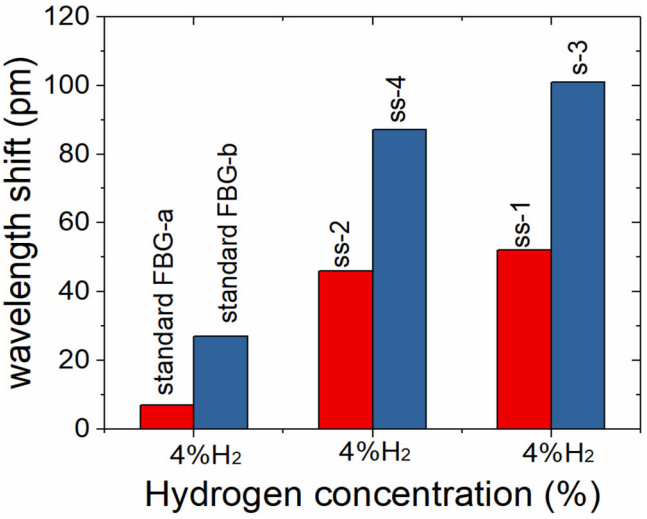

Figure 8. Wavelength shifts of sensors coated with Pd_4/Ag_1 and Pd_{87}/Ni_{13} film.

4.4. Effect of Temperature on Hydrogen Probe

As demonstrated in Fig. 7(a), the center wavelength shift of sample s-3 is 107 pm and 100 pm toward 4%, 4% H_2 at 25 °C, respectively. When the testing temperature rises to 50 °C, the hydrogen response cycle test of sample s-3 at 4% H_2 is shown in Fig. 8. The central wavelength shifts were 372 pm, 370 pm and 370 pm at three cycles of hydrogen gas test, respectively, as shown in Fig. 9. It can be observed that, at the beginning and the end of each cycle, large fluctuation of wavelength occurs. This phenomenon is related to the change in the testing environment. When the gas chamber cover was completely opened, the change of gas pressure and temperature caused the central wavelength to experience a sharp rise and fall. Similarly, when the gas chamber was closed, the central wavelength also underwent a sudden change due to the variation of air pressure. However, this did not affect the testing result of the sensing probe.

Comparing the performance of the samples at different temperatures, it can be seen that the sensitivity and repeatability of the probes have greatly improved. This is attributed to several reasons: firstly, an increase in temperature leads to an increase in kinetic energy of the molecules. After the hydrogen is absorbed by the palladium membrane, it decomposed into H atoms. Owing to higher temperature, the hydrogen atoms can penetrate deep into the film, and the water molecules adsorbed on the surface of the film are discharged, which enhances the penetration of hydrogen atoms. The increased repeatability of the probes is due to the annealing effect. When the sample is placed in a closed testing chamber and annealed 50 °C, this process effectively improves the reproducibility of palladium alloy in a hydrogen sensor [18]. Low-temperature annealing can improve the grain structure of palladium alloy and eliminate intergranular defects deposited during coating, such as residual stress. During the hydrogen test, the samples are always placed in a low-temperature annealing environment, which can effectively avoid some defects such as the phase transition and lattice deformation of the palladium membrane after hydrogen absorption.

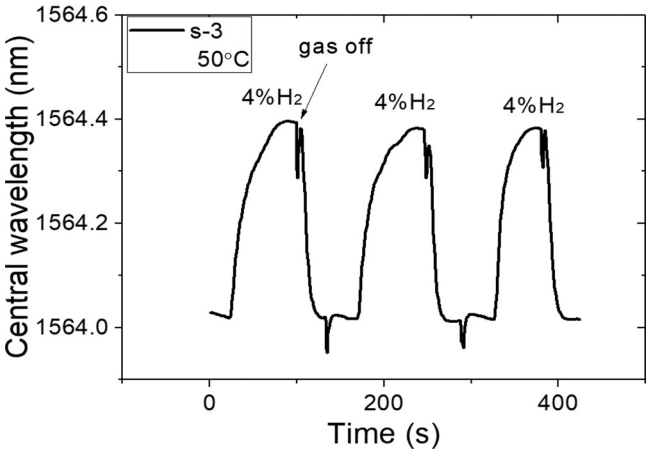

Figure 9. The hydrogen response of sample s-3 at 50 °C.

5. Conclusion

Effective use of fs laser ablation to machine spiral microgroove on the fiber cladding coupled with magnetron sputtering of 520 nm thickness of Pd_{83}/Ni_{17} and Pd_4/Ag_1 composite thin film enhances sensor performance. The surface morphology, the content of elements and structure of cross-section was analyzed by XRD, EDS and SEM. The crystal lattice of Pd_{87}/Ni_{13} alloy film shrunk. The response time was about 80 s and the recovery time was faster than response time. The single and double spiral microstructured FBG sensor was tested in hydrogen gas using air as carrier gas at room temperature. The double spiral probe had the highest sensitivity, followed by a single spiral sensor and standard FBG sensor. Comparing probes coated with Pd_{87}/Ni_{13} film and Pd_4/Ag_1 composite films, the latter has higher sensitivity. Increased temperature improved the sensitivity and repeatability of probes due to annealing effects. The laser power had a strong effect on the performance of the sensors. All spiral sensors showed reversible and higher sensitivity compared to standard FBG sensor.

Funding

This work was supported by the National Natural Science Foundation of China under grant 51975192, 51975442, the Natural Science Foundation of Hubei Province under grant 2019CFB632, and the Ph.D. Research Fund of Hubei University of Arts and Science (No. 2059016), Hubei Superior and Distinctive Discipline Group of "Mechatronics and Automobiles" (XKQ2021050).

References

1. Y. Wang *et al.*, Temperature-insensitive current sensor using two cascaded FBGs, *Integr. Ferroelectr.* **190** (1), 120 (2018). DOI: 10.1080/10584587.2018.1457345.
2. H. Lu *et al.*, Pd and Pd-Ni alloy composite membranes fabricated by electroless plating method on capillary α-Al_2O_3 substrates, *Int. J. Hydrogen Energy* **40** (8), 3548 (2015). DOI: 10.1016/j.ijhydene.2014.09.121.

3. Y. J. Ou *et al.*, Nanostructures of Pd–Ni alloy deposited on carbon fibers for sensing hydrogen, *J. Alloy Compd.* **569** (12), 130 (2013). DOI: 10.1016/j.jallcom.2013.03.180.
4. J. Dai *et al.*, Greatly etched fiber Bragg grating hydrogen sensor with Pd/Ni composite film as sensing material, *Sens. Actuators B Chem.* **174** (11), 253 (2012). DOI: 10.1016/j.snb.2012.07.018.
5. E. Lee *et al.*, Pd–Ni hydrogen sponge for highly sensitive nanogap-based hydrogen sensors, *Int. J. Hydrogen Energy* **37** (19), 14702 (2012). DOI: 10.1016/j.ijhydene.2012.07.004.
6. Y. K. Gautam *et al.*, Studies on hydrogen sensing properties of nanostructured Pd and Pd/Mg thin films prepared by pulsed laser deposition, *Sens. Actuators B Chem.* **176**, 453 (2013). DOI: 10.1016/j.snb.2012.09.065.
7. M. Slaman, Optimization of Mg-based fiber optic hydrogen detectors by alloying the catalyst, *Int. J. Hydrogen Energy* **33** (3), 1084 (2008). DOI: 10.1016/j.ijhydene.2007.09.036.
8. D. Luna-Moreno and D. Monzón-Hernández, Effect of the Pd-Au thin film thickness uniformity on the performance of an optical fiber hydrogen sensor, *Appl. Surf. Sci.* **253** (21), 8615 (2007). DOI: 10.1016/j.apsusc.2007.04.059.
9. C. V. Miguel *et al.*, Effect of CO and CO_2 on H_2 permeation through finger-like Pd-Ag membranes, *Int. J. Hydrogen Energy* **37** (17), 12680 (2012). DOI: 10.1016/j.ijhydene.2012.05.131.
10. Z. Yu *et al.*, Highly sensitive fiber taper interferometric hydrogen sensors, *IEEE Photonics J.* **8** (1), 1 (2016). DOI: 10.1109/JPHOT.2015.2507369.
11. S. Silva *et al.*, H_2 sensing based on a Pd-coated tapered-FBG fabricated by DUV femtosecond laser technique, *IEEE Photon. Technol. Lett.* **25** (4), 401 (2013). DOI: 10.1109/LPT.2013.2239985.
12. D. Zalvidea *et al.*, Hydrogen sensor based on a palladium-coated fibre-taper with improved time-response, *Sens. Actuators B Chem.* **114** (1), 268 (2006). DOI: 10.1016/j.snb.2005.05.010.
13. J. Jiang *et al.*, Highly sensitive dissolved hydrogen sensor based on side-polished fiber Bragg grating, *IEEE Photon. Technol. Lett.* **27** (13), 1453 (2015). DOI: 10.1109/LPT.2015.2425894.
14. C. Tien *et al.*, Hydrogen sensor based on side-polished fiber bragg gratings coated with thin palladium film, *Thin Solid Films* **516** (16), 5360 (2008). DOI: 10.1016/j.tsf.2007.07.045.
15. M. Zou *et al.*, Femtosecond laser ablated FBG with composite microstructure for hydrogen sensor application, *Sensors* **16** (12), 2040 (2016). DOI: 10.3390/s16122040.
16. L.-G. Petersson, H. M. Dannetun, and I. Lundström, Hydrogen detection during catalytic surface reactions: Evidence for activated lateral hydrogen mobility in the water-forming reaction on Pd, *Phys. Rev. Lett.* **52** (20), 1806 (1984). DOI: 10.1103/PhysRevLett.52.1806.
17. J. Dai *et al.*, Enhanced sensitivity of fiber Bragg grating hydrogen sensor using flexible substrate, *Sens. Actuators B Chem.* **196**, 604 (2014). DOI: 10.1016/j.snb.2014.02.069.
18. C. Wadell *et al.*, Hysteresis-free nanoplasmonic Pd–Au alloy hydrogen sensors, *Nano Lett.* **15** (5), 3563 (2015). DOI: 10.1021/acs.nanolett.5b01053.